Optical Engineering

OpticalEngineering.SPIEDigitalLibrary.org

Design and implementation of three-dimensional ring-scanning equipment for optimized measurements of near-infrared diffuse optical breast imaging

Jhao-Ming Yu
Min-Cheng Pan
Ya-Fen Hsu
Liang-Yu Chen
Min-Chun Pan

SPIE.

Design and implementation of three-dimensional ring-scanning equipment for optimized measurements of near-infrared diffuse optical breast imaging

Jhao-Ming Yu,[a] Min-Cheng Pan,[b] Ya-Fen Hsu,[c] Liang-Yu Chen,[d] and Min-Chun Pan[a,d,*]
[a]National Central University, Department of Mechanical Engineering, No. 300, Zhongda Road, Zhongli District, Taoyuan City 320, Taiwan
[b]Tungnan University, Department of Electronic Engineering, No. 152, Sec. 3, Beishen Road, Shenkeng District, New Taipei City 222, Taiwan
[c]Landseed Hospital, Department of Surgery, No. 77, Guangtai Road, Pingzhen District, Taoyuan City 324, Taiwan
[d]National Central University, Graduate Institute of Biomedical Engineering, No. 300, Zhongda Road, Zhongli District, Taoyuan City 320, Taiwan

Abstract. We propose and implement three-dimensional (3-D) ring-scanning equipment for near-infrared (NIR) diffuse optical imaging to screen breast tumors under prostrating examination. This equipment has the function of the radial, circular, and vertical motion without compression of breast tissue, thereby achieving 3-D scanning; furthermore, a flexible combination of illumination and detection can be configured for the required resolution. Especially, a rotation-sliding-and-moving mechanism was designed for the guidance of source- and detection-channel motion. Prior to machining and construction of the system, a synthesized image reconstruction was simulated to show the feasibility of this 3-D NIR ring-scanning equipment; finally, this equipment is verified by performing phantom experiments. Rather than the fixed configuration, this addressed screening/diagnosing equipment has the flexibilities of optical-channel expansion for spatial resolution and the dimensional freedom for scanning in reconstructing optical-property images. [DOI: 10.1117/1.OE.54.7.073107]

Keywords: three-dimensional ring-scanning equipment; near-infrared diffuse optical imaging; breast tumor.

Paper 141906 received Dec. 15, 2014; accepted for publication Jun. 19, 2015; published online Jul. 23, 2015.

1 Introduction

X-ray mammography for clinical breast examination is currently one of the standard operation routines of screening breast cancer; normally, ultrasound imaging (UI) and magnetic resonance imaging (MRI) are used clinically to clarify suspicious results detected by mammograms.[1] Even x-ray mammography for microcalcifications has a reliable detection capability, but it does not avoid the high false-negative results of screening breast tumors and harmful radiation in spite of the small dose. Compared with x-ray mammography, UI and MRI can show the physiological information of breast tissue and provide functional imaging. However, the screening through UI is quite dependent upon the operation, and thus various outcomes result from operators' procedures; furthermore, MRI is expensive and is usually employed together with a contrast agent for better results.[2]

Diffuse optical imaging (DOI) providing functional information of tissues has drawn great attention for the last two decades,[3] which is a functional, nonradioactive, and comparatively cost-effective imaging technique. Composed of a photoelectric measuring module of source-and-detection, scanning equipment, system control, and data processing of image reconstruction, near-infrared (NIR) DOI systems are developed for the screening and diagnosis of breast tumors. In NIR DOI systems for the screening and diagnosis of breast tumor, their scanning mechanisms can be mainly divided into two categories, i.e., flat compression and circular arrangement modes;[4,5] the former resembles mammography using two movable compression plates and the latter primarily adopts a fixed architecture. In the circular arrangement mode, a special type of jaw- or cup-shaped design was implemented[6,7] with one or more layers of fixed source-and-detection channels in a circle. Focusing on the scanning mechanisms, a systematic review is illustrated in Table 1,[5–23] which summarizes the varied designs of the measuring module in terms of (1) the scheme of source-and-detection configuration, (2) the mechanism type, and (3) signal characteristics of NIR data. Also, the definitions of abbreviations used in Table 1 are stated in the table footnote.

Typically, the scanning equipment belonging to fixed source-and-detector configuration limits the resolution of reconstructed tomographical images to an extent.[24,16] To cope with the issue, a flexible ring-scanning mechanism design has been investigated and analyzed in order to obtain best effectiveness and efficiency while retaining an acceptable scanning time.[25]

In this previous study, associated with the expected scanning time and the corresponding reconstructed images based on the finite element method (FEM), varied illumination-and-detection combinations have been simulated and discussed, thereby yielding a suitable design in terms of operation time and image quality. In the design of optical channel configuration, the circular scanning module is divided into m zones, and each zone includes n NIR sources and l detection fibers, denoted as mZnS. For example, it is referred to as 2Z3S provided that a circumference is divided into two zones and

*Address all correspondence to: Min-Chun Pan, E-mail: pan_minc@cc.ncu.edu.tw

0091-3286 /2015/$25.00

Table 1 Literature review for varied designs of the measuring module in the near-infrared (NIR) diffuse optical imaging (DOI) system.

	Mechanism design					Illumination and detection			
Years	Source-detection scheme[a,b]	Type[c]	Contact	Scanning	Size adjust	DC/FD/TD[d]	Wavelength (nm)	Scattering liquid added	References
1997	16S + 16D → 16S × 16D	R	Y	N	N	FD (100 MHz)	800	N	5
1997	1S + 16D (fan) →16S × 16D	R	N	Y	N	TD (160 fs)	780	N	8
1999	256SD (3-D) → 256S × 255D	B	N	N	N	DC	660, 780, 920	Y	9
2000	32S + 32D → 32S × 32D	R	Y	N	N	TD (500 ps)	800	N	10
2001	16S + 16D → 16S × 16D	R	Y	N	Y	FD (100 MHz)	750, 800	N	11
2002	16S + 16D → 16S × 16D	R	Y	N	Y	FD (100 MHz)	761, 785, 808, 826	N	12
2003	16S + 16D → 16S × 16D × 3L	R	Y	N	Y	FD (100 MHz)	761, 785, 808, 826	N	13
2003	16S + 16D → 16S × 16D × 4L	R	Y	N	Y	DC	785, 808, 830	N	14
2005	31SD (3-D) → 31S × 30D	B	N	N	N	TD	780, 816	Y	15
2006	8S + 8D → 8S × 8D	R	Y	N	Y	FD (110 to 280 MHz)	665, 785, 800, 830	N	16,17
2008	16SD → 16S × 11D (fan)	R	Y	Y	Y	DC	805	N	18
2008	253S + 254D (3-D) → 253S × 254D	B	N	N	N	DC	690, 730, 780, 850	Y	7
2009	16SD → 16S × 15D	R	N	Y	Y	DC	800	N	19
2009	20SD → 20S × 19D	R	Y	Y	Y	FD (100 MHz)	785	N	20
2011	16S + 16D → 16S × 16D	R	Y	N	Y	DC	775	N	21
2011	(16S + 16D) × 2 (3-D) → 32S × 64D	P	Y	N	Y	DC	765, 808, 827, 805	N	6 and 22
2013	96SD (for 4L)→32S × 64D	R	Y	N	Y	FD (5 kHz, 7 kHz)	765, 808, 827, 905	N	23

[a] *n*S + /D means there are *n* sources and *l* detectors in the measuring device, thereby leading to the acquired data of *n*S × /D combinations; *k*SD indicates there are *k* sources and detectors in total with illumination and detection being flexibly switched between each other; L represents the measured layers.
[b] 3-D in parentheses indicates that sources and detectors were distributed over a three-dimensional cup.
[c] R, ring; B, bra shape; P, palm claw.
[d] DC, direct current NIR; FD, frequency domain (or amplitude modulated) NIR; TD, time domain (or pulsed) NIR.

each zone has three source fibers and 15 detection fibers; i.e., there are six for illumination and 30 for detection in total. Owing to the space limitation and the physical dimension of illumination and detection fiber heads, 36 illumination and detection channels are adopted, and thus, two heads are arranged in a 10 deg separation. From the simulation, the 2Z3S or 3Z3S configuration was found to be an apparently better design for the ring-scanning mechanism in terms of both the resolution of those reconstructed optical property images and the scanning time of equipment.

In this paper, we propose and implement a rotating ring-scanning mechanism for a three-dimensional (3-D) NIR DOI system for prostrating examination with flexible combinations of illumination and detection channels and without the compression of breast tissue. Following that, the detailed mechanism design is considered in the 3-D architecture, i.e., the radial, angular, and vertical directions. The scanning equipment is limited by the physical dimension of illumination and detection fibers; 36 fibers in total are arranged in the circumference of a layer. Moreover, a predefined microscanning can be performed as required, thereby obtaining a high spatial resolution and thus a high spatial-frequency resolution.

Following the aforementioned introduction, this paper is organized as follows. In Sec. 2, simulation verification prior to system machining and construction is performed by synthesized images in cases of (1) 3-D reconstruction and (2) comparison between ring-scanning and fixed-channel mechanisms. In Sec. 3, we discuss the design of the 3-D ring-scanning mechanism where the radial motion of optical source/detector channels is further investigated in detail; additionally, component specification and dimension constraints for the machining are presented. Subsequently, Sec. 4 discusses and illustrates the operation time of ring scanning in a 3-D track, and system control issues on mechanical motion and opto-electrical measurement; furthermore, experimental validation is presented. Finally, Sec. 5 gives concluding remarks.

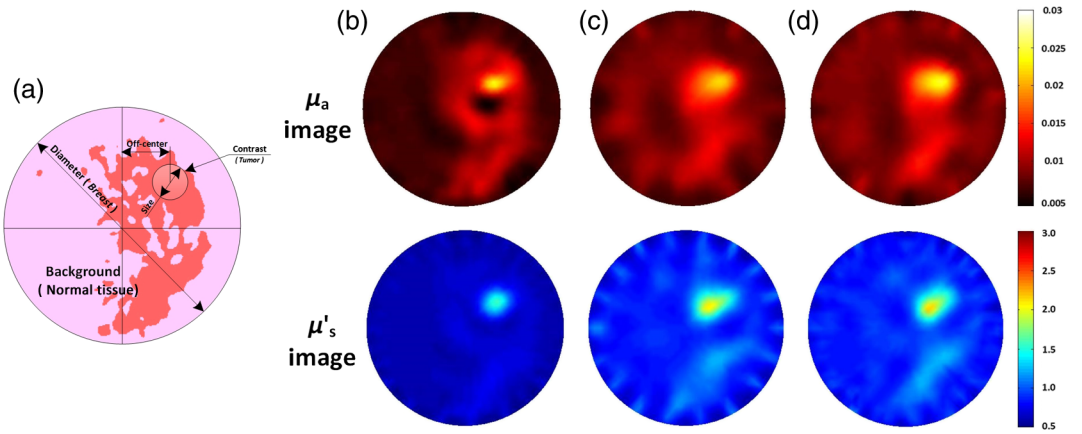

Fig. 1 Comparison between the fixed-channel and the proposed 2Z3S design. (a) Synthesized phantom image with an inclusion added, and the reconstructed μ_a and μ_s' images of (b) the fixed-channel design (18S + 18D), and (c) 18 and (d) 36 optical channels used in total for the proposed 2Z3S design, respectively.

2 Simulation Verification Prior to System Construction

Prior to the construction of manufacturing, simulation was first performed to verify the feasibility of our 3-D ring-scanning equipment. Comparison between a ring-scanning and a fixed-channel mechanism was conducted and the reconstruction for synthesized images in 3-D as shown in Sec. 2.1.[26]

2.1 *Comparison Between a Ring-Scanning and a Fixed-Channel Mechanism*

To illustrate the performance of the proposed ring-scanning equipment, a computational case study was performed. A self-coded computer program for image reconstruction in the frequency domain, named NIR.FD_PC, was used, which was based on FEM and incorporated with Tikhonov regularization.[27]

In the simulation case, a 10-mm-diameter inclusion in an 80-mm-diameter background tissue is assumed; the contrast of inclusion-to-background is 3, where μ_a and μ_s' of the background are 0.01 and 1.0 mm^{-1}, respectively; also, the inclusion location is shown as Fig. 1(a). This original cross-section image was obtained with slicing a 3-D breast MRI from Taipei Medical University Hospital thereafter. Comparison is made between a fixed-type (18S + 18D) and a ring-scanning configuration; illumination and detection of the former are fully arranged in turn and those of the latter are arranged as 2Z3S; Fig. 2 clearly demonstrates the operation of the so-called 2Z3S configuration. Figure 1 illustrates two sets of reconstructed μ_a and μ_s' images as shown in the up and down row, respectively, resulting from the mechanisms of the fixed-channel type [Fig. 1(b)] and 2Z3S configuration [Figs. 1(c) and 1(d)] associated with 18 and 36 optical channels in total, respectively. Here, Fig. 1(b) obtained by the fixed channel configuration shows a clearer μ_s' image than Figs. 1(c) and 1(d) from the ring-scanning one, but μ_a images are noticeable in the latter. For the functional medical imaging, μ_a images are even more important than μ_s' images. Compared with the result using 18 optical channels [Fig. 1(c)], the image using 36 optical channels [Fig. 1(d)] has higher contrast for the μ_a image and less ringing artifacts for the μ_s' image. Therefore, as to the performance of image reconstruction, Figs. 1(c) and 1(d) are still competitive to Fig. 1(b); it reveals that the ring-scanning configuration proposed here can be adopted, although the fixed-channel type has been frequently used.

2.2 *Reconstruction for Synthesized Images in 3-D*

Furthermore, a computational case study was synthesized to illustrate image reconstruction through our proposed 3-D scanning. Figure 3 illustrates the scanning of three cross-sections and their reconstructed μ_a and μ_s' images, where the optical property coefficients are same as Fig. 1(a). In the simulation case, a 10-mm-diameter inclusion in an

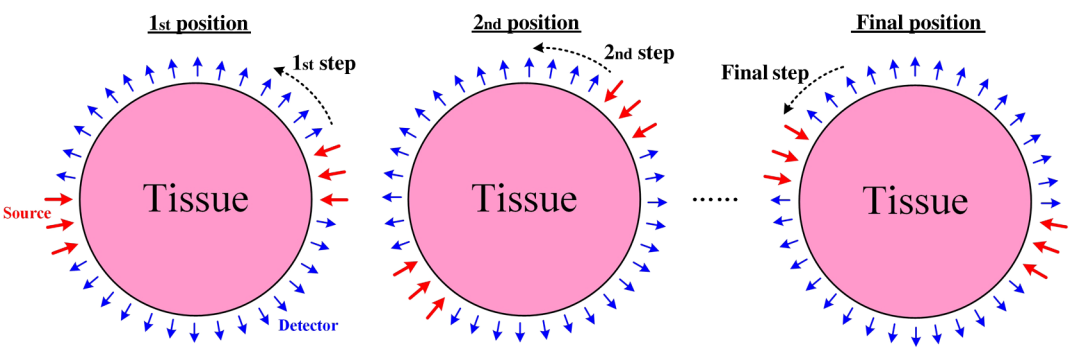

Fig. 2 Schematic of the ring-scanning operation for 2Z3S configuration.

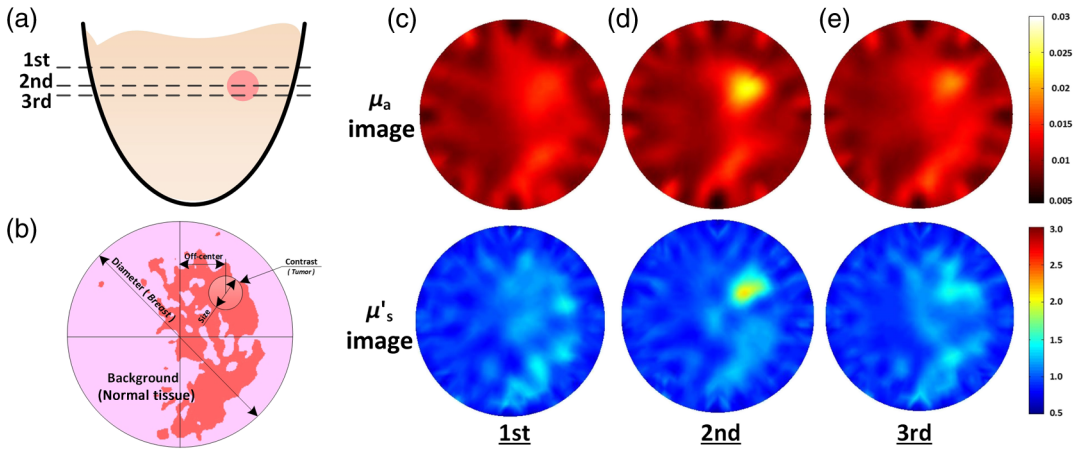

Fig. 3 Illustration of a synthesized diffuse optical imaging (DOI) image reconstruction through the three-dimensional (3-D) scanning: (a) the positions of three slices in the simulated breast, (b) second slice breast diagram, and reconstructed optical property images of (c) first slice, (d) second slice, and (c) third slice.

80-mm-diameter background tissue was assumed; the second section cut through the center of inclusion, and the first and third sections went beyond the inclusion and through the lower part of inclusion, respectively. As shown in Fig. 3, the reconstructed images from these three slices are illustrated in Figs. 3(c), 3(d), and 3(e), respectively; it can be seen that Fig. 3(d) shows a clear inclusion rather than Figs. 3(c) and 3(e), thereby implying the resolution ability of the proposed configuration for varied inclusions.

It is worth emphasizing that the proposed 3-D ring-scanning equipment for screening/diagnosing breast tumor has the potential and flexibility of optical channel expansion by user-defined half-span (or less one span) scanning through circular motion, which is not achieved by using the design of a fixed-channel configuration.

3 Design of 3-D Ring-Scanning Mechanism

In this section, movement mechanism in 3-D directions is generally described. Especially, the mechanism is further investigated for radial movement of optical source and detector channels; subsequently, practical design parameters are discussed in the consideration of the specifications of fibers used and the physical dimension of breasts.

A ring-scanning-based architecture for the NIR DOI system was proposed, designed, and developed for the screening and diagnosis of breast tumors. Figure 4 shows a system schematic, the dedicated design of which has the following benefits besides avoiding discomfort through prostrating examination.

1. Compromise between efficiency and effectiveness: the ring-scanning design takes a trade-off between reconstructed image quality and scanning time,[25]
2. Flexibility: adjustable scanning range for various breast sizes and cross-sections through a dedicated design with the rotation-sliding-and-moving mechanism, and
3. Varying detection-channel numbers: varying channel numbers dependent upon breast/phantom size to enhance spatial resolution.

Figure 5 illustrates the design of the 3-D ring-scanning mechanism with illumination and detection fiber channels, which mainly includes (1) a dedicated rotating disk using a stepping motor A to drive illumination and detection fibers simultaneously in the radial direction, (2) both a stepping motor B and a speed-reduction bevel gear box to provide circular movement, and (3) a motor C and a linear ball screw to offer vertical movement.

1. Radial motion: To accommodate various breast sizes for screening, a dedicated disk platform with illumination and detection fiber channels is driven by a V-belt set to achieve the radial movement of all channels. These fiber channels are driven to move in the radial

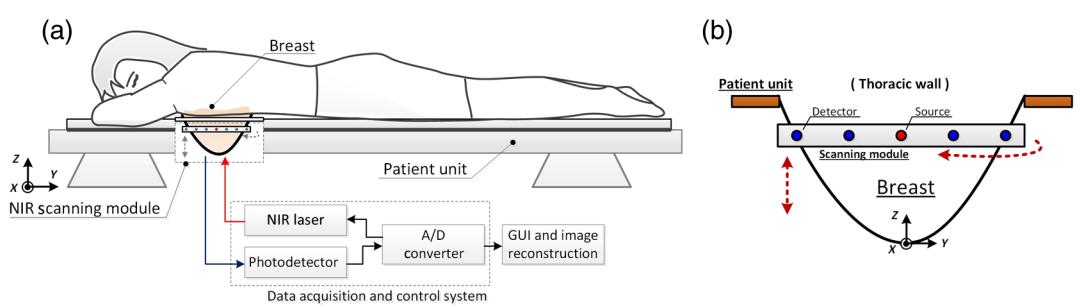

Fig. 4 Schematic diagrams of (a) a prostrating NIR DOI system, and (b) zoom-in illustration for breast tumor detection.

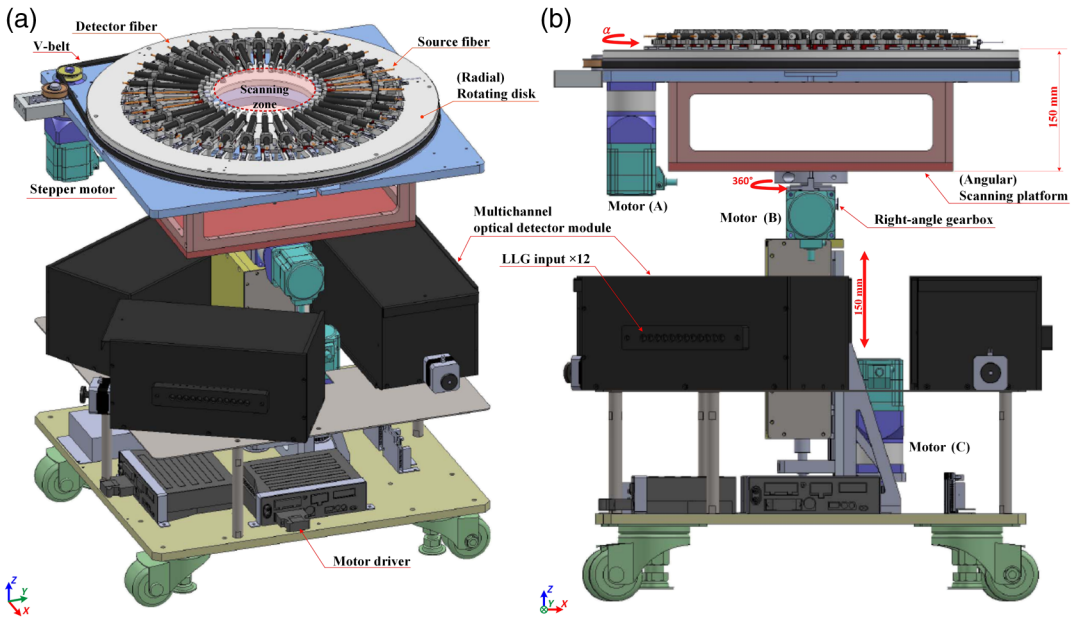

Fig. 5 Illustration of scanning mechanism for 3-D imaging; (a) an overview and (b) a side view to illustrate its movement.

direction until a predefined gap to the breast, which are guided and decided by three optical displacement sensors.

2. Circular motion: To achieve the ring scanning, a stepping motor B installed under the disk platform connects to a bevel gearbox with a speed reduction ratio 2 for a smooth drive, as shown in Fig. 5. The ring-scanning angle can be as high as 360 deg, depending on which illumination-and-detection configuration is used; for instance, the angle is 150 deg for the 2Z3S configuration.[25]
3. Vertical motion: To acquire optical data for various cross-sections of a breast, the disk platform can move vertically by using a linear ball screw driven by a timing belt connected to a stepping motor C, the movable distance of which can be up to 150 mm.

For the estimation of each scanning profile, three optical displacement sensors are used such that it enables a noncontact or soft-touch NIR data acquisition for image reconstruction. Moreover, several limit switches are mounted at the end of the movement stroke for safety reasons, such as one for circular movement, two for vertical movement on the upward and the downward ends, and two at the photomultiplier tube (PMT) translation stage. The operation to complete a 3-D movement of the scanning system is controlled by using a mainframe computer through a data acquisition/motion control card and a coded user interface in LabVIEW®.

3.1 *Mechanism for Radial Movement of Optical Source-and-Detector Channels*

Composed of a rotating disk platform with a belt idler pulley, a V-belt pulley, and a V-belt, a rotation-sliding-and-moving mechanism was designated to drive the entire 36 optical illumination-and-detection channels for radial movement, as shown in Fig. 6. The detailed description is described as follows.

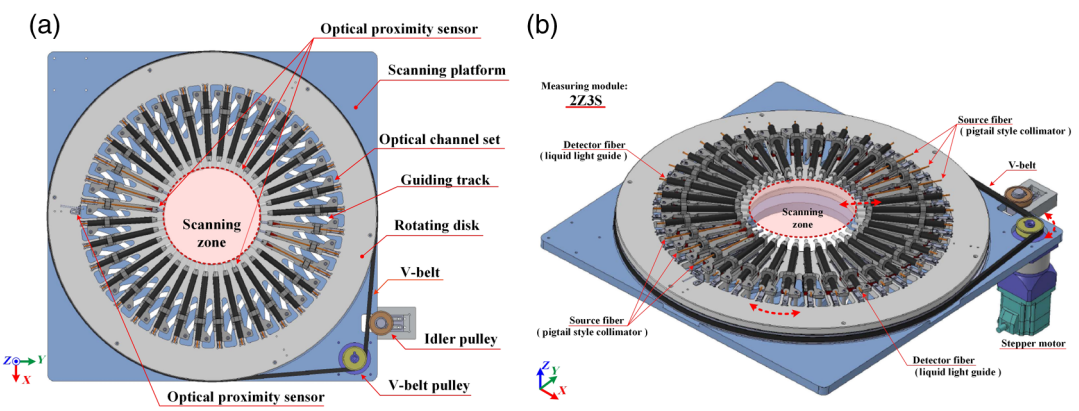

Fig. 6 Schematic of the radial-movement mechanism for optical illumination-and-detector channels: (a) top view and (b) bird's eye view.

Figure 7 shows a schematic of the design of a single optical channel in radial movement, where α is the drive angle for the rotation angle of the rotating disk as the light guide reaches a radial distance ΔL_α, β is the lead angle between the light guide and the guiding track, δ is the offset distance between the connecting rod and the light guide, and l_T is the track length; in addition, L and $\Delta L_{\max}$ are the length of a fiber holder and the maximum distance of radial movement, respectively. Compared with fiber bundles, liquid light guides (LLG, 77635 Newport Corporation) are useful, of which the core, numerical aperture, acceptance cone, and minimum bend radius are equal to 3 mm, 0.52, 62 deg, and 40 mm, respectively. From the light guide number, N, and LLG diameter, D_{LLG}, the minimum scanning diameter, $D^{\mathrm{min}}_{\mathrm{breast}}$, can be determined as Eq. (1), and thus $\Delta L_{\max}$ is the difference of $D^{\mathrm{max}}_{\mathrm{breast}}$ and $D^{\mathrm{min}}_{\mathrm{breast}}$, as in Eq. (2). The radial displacement ΔL_α can be expressed as Eq. (3) in terms of α, β, δ, l_T, and L.

$$D^{\mathrm{breast}}_{\mathrm{min}} = (D_{\mathrm{LLG}}) \cot\left(\frac{\pi}{N}\right), \tag{1}$$

$$\Delta L_{\max} = \frac{(D^{\mathrm{breast}}_{\max} - D^{\mathrm{breast}}_{\mathrm{min}})}{2}, \tag{2}$$

$$\Delta L_\alpha = L \cos\alpha - \delta \sin\alpha - L + K_\alpha l_T \cos\beta \, K_\alpha = \alpha/\alpha_{\max}, \tag{3}$$

where K_α ranges between [0, 1] in proportion to the drive angle α; for instance, K_α equals 1 as α reaches to its maximum. As can be seen in Eq. (3), ΔL_α varies with the driving angle α that is dependent upon the designated lead angle β. According to the further analysis of Eq. (3), β ranges from 10 to 75 deg such that it enables to avoid self-locking or moving hysteresis when the light guide unit slides in the guiding track. Here, β is designated as 35 deg for the link of an optical channel set smoothly moving in the track (explained further next).

Figure 8 shows that the radial movement of each optical channel set operates through a radial guiding track and a link of light guide unit. Figure 8(d) illustrates the detail of a single optical channel set that is composed of an illumination optical fiber [Fig. 8(a)] or a detection LLG [Fig. 8(b)], a light guide unit with two fiber holders, and a linear guideway connected to the link incorporated with the rotating disk platform. In addition, Fig. 8(c) shows that a bearing used as a sliding wheel was installed at the lower end of the link. The LLG (or fiber) is fixed by two fiber holders at the light guide unit, which is connected with the link for rotational sliding to move radially with the help of the linear guideway. As shown in Fig. 6(b), the V-belt powered by the stepper motor drives the rotating disk platform to guide the optical channel set moving in the radial direction as explained in Fig. 7.

Furthermore, the optimal driving angle (α) and the lead angle (β) are analyzed through Eq. (3) as K_α equal to 1 and charted in Fig. 9; it can be seen how the maximum distance of radial movement ($\Delta L_{\max}$) is affected by α and β. It is noted in Fig. 9(a) that the corresponding radial movement, ΔL_α, varies slightly along the changing of β as it is smaller than 10 deg and the self-locking occurs as β is >75 deg. Considering that $\Delta L_{\max}$ is designated as 50 mm such that α and β should be ranging between [15 deg, 20 deg] and [30 deg, 40 deg], respectively, as can be seen in Fig. 9(b). In the current design, α and β are designated as 17 and 35 deg, respectively.

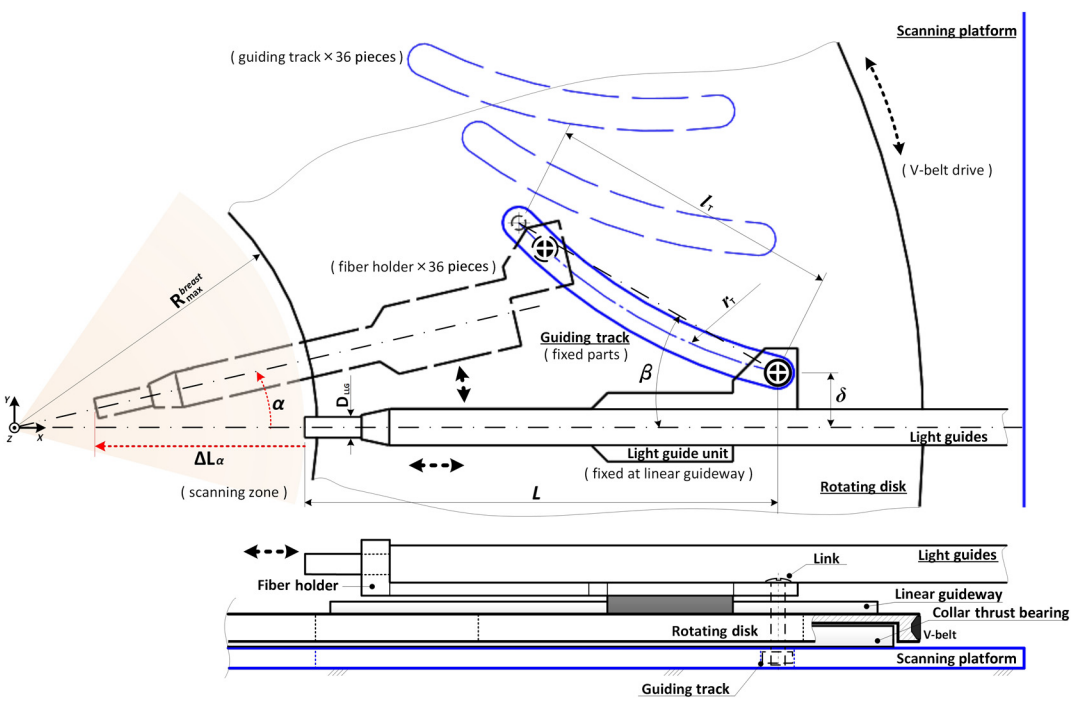

Fig. 7 Illustration of the design of a single optical channel in radial movement.

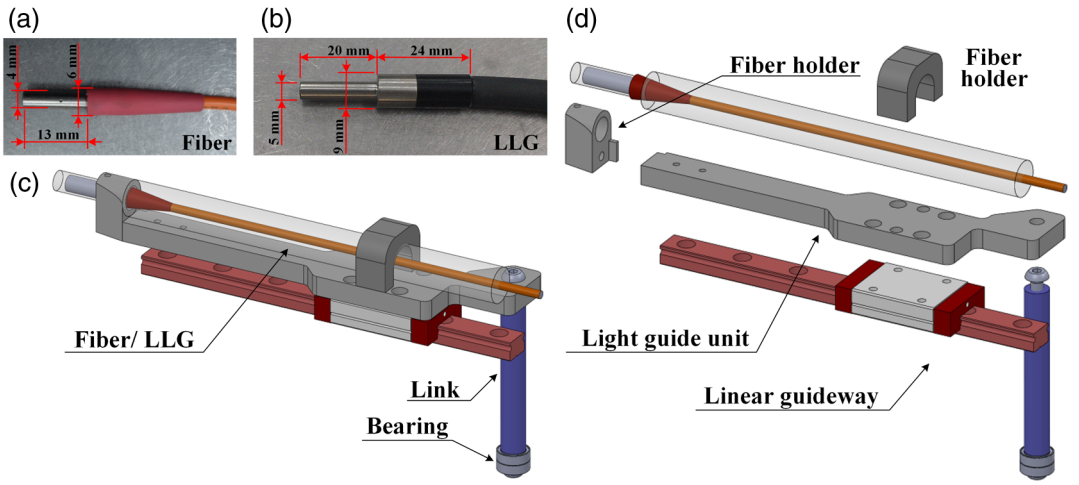

Fig. 8 Detailed design of a single optical channel set; (a) illumination fiber, (b) detection fiber-LLG, (c) schematic diagram of a single optical channel set, and (d) its exploded view.

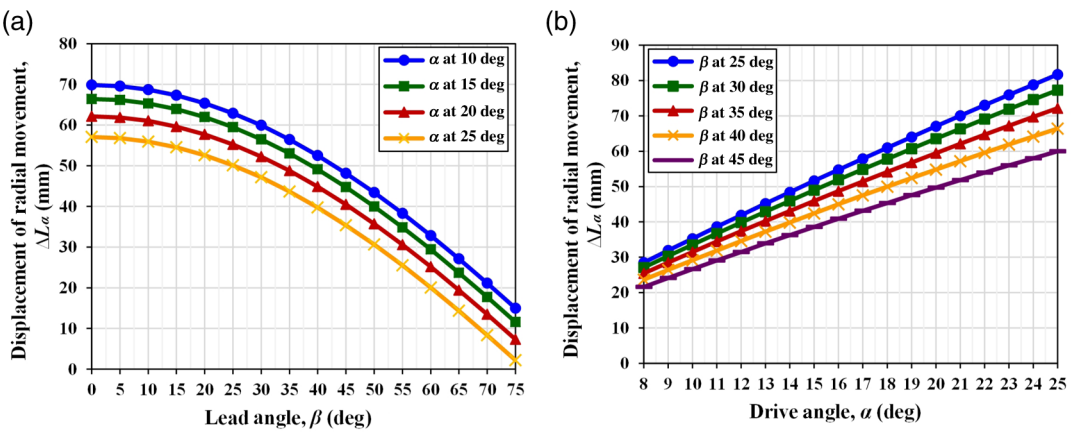

Fig. 9 Illustration of radial displacement relating to (a) lead angle β and (b) drive angle α.

3.2 *Design in the Consideration of Screened Breast to be Accommodated*

The ring-scanning-based measuring equipment employs commercially available optical fibers and LLGs for source illumination and diffused-light collection. To be applied in the screening and diagnosis of human breasts, the physical dimensions of the breast to be screened and both optical fibers and LLGs used were considered during the design phase. Table 2 lists the important specifications of LLGs used and the corresponding features. As shown in Table 2, the diameter of the core (3 mm) plus the shell of an LLG equals 5 mm (D_{LLG}) such that the number (N) of LLGs being used is 36 at maximum; therefore, the breast dimension (D_{breast}) to be accommodated here ranges from 60 ($D_{\mathrm{breast}}^{\mathrm{min}}$) to 150 mm ($D_{\mathrm{breast}}^{\mathrm{max}}$) in diameter. In the state of $D_{\mathrm{breast}}^{\mathrm{max}}$, α_{max}, β, and δ correspond to the values of 17 deg, 35 deg, and 13.5 mm in the bench. Following the aforementioned specification, the design yields L and l_T of 120 and 74 mm, respectively. All these values were used as the initial conditions for the computer-aided design model to complete the detail design of each machine part of the prototype equipment. It should be noted that in the design driving a radial movement may cause an angular shift of α in the set of LLGs. Therefore, angle compensation is performed prior to each radial movement. Table 2 lists the design parameters and their specification of the diffuse optical tomography test bench. Three sets of proximity sensors (650 nm, HPX-EG00-1S, Azbil corporation) were mounted along the illumination-detection ring evenly for two purposes: (1) to estimate breast contour in the scanning plane for the modeling of image reconstruction and (2) to protect the patients to be screened through lightly touching tissue of all illumination-detection optical fibers and LLGs. It is noted that the proximity sensors are activated only when the radial movement is in progress.

Table 2 Design parameters and their specification of diffuse optical tomography test bench.

Specification	N	L	D_{LLG}	l_T
Value	36	120 mm	5 mm	74 mm
Specification	$D_{\mathrm{breast}}^{\mathrm{max}}$	δ	α_{max}	B
Value	150 mm	13.5 mm	17 deg	35 deg

Note: The values of δ, α_{max}, and β determined with $D_{\mathrm{breast}}^{\mathrm{max}}$.

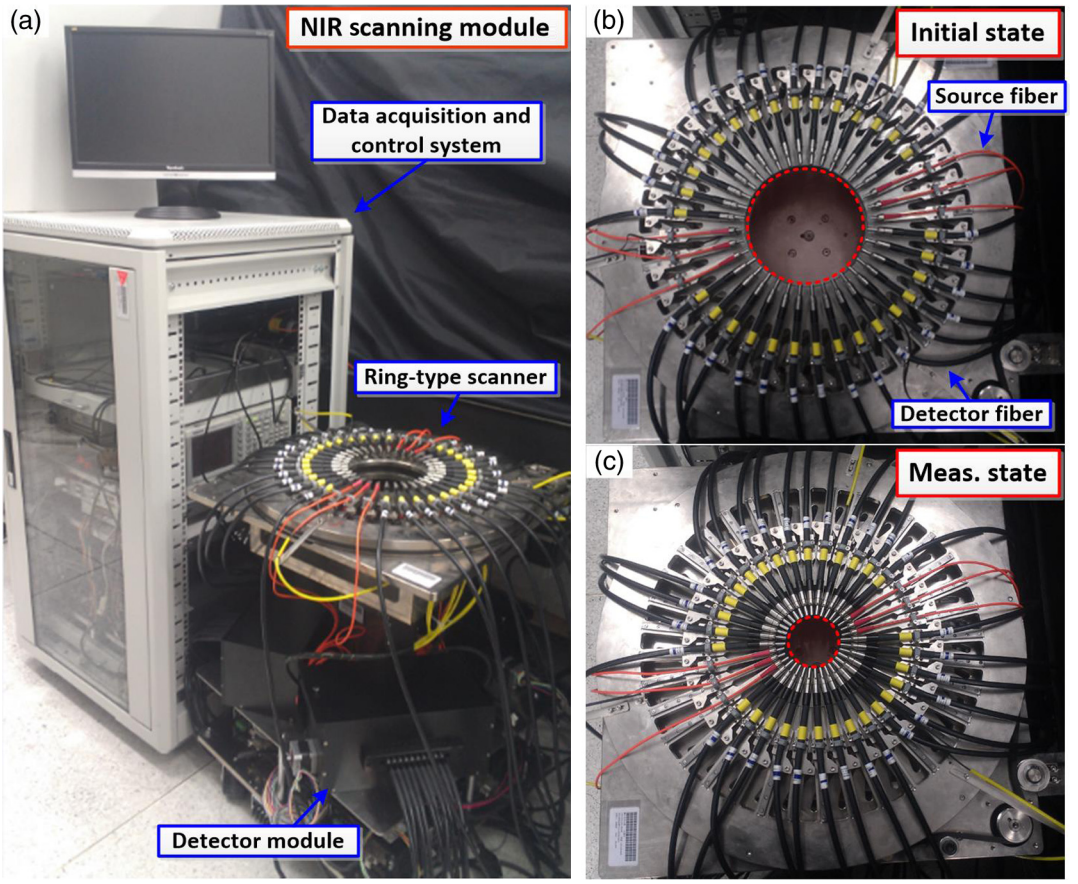

Fig. 10 Demonstration of (a) the prototype instrument at (b) an initial state or (c) a measuring state.

4 Evaluation and Discussion

Based on the synthesized design with acceptable scanning time and simulated image quality,[25] the prototype ring-scanning equipment was machined and assembled (Fig. 10) to conduct experiments for acquiring NIR data and reconstructing images. Using this prototype equipment for NIR DOI, the experimental scenarios are designated as follows.

1. As a subject to be screened or diagnosed lies on the bench to enable the breast to suspend in the scanning zone, the optical channels are radially driven close to the chest wall with the help of the round rotating disk and the optical proximity sensors.
2. Subsequently, the ring-scanning module is driven counterclockwise with the square scanning platform to rotate an interval of 30 deg, e.g., for the 2Z3S configuration;[25] as soon as the out-emitting NIR radiance is acquired for the completion of 150 deg circular movement, the module stops rotating.
3. Finally, the module returns to the starting point and also back to the position of maximum radial dimension as the ring-scanning module completes the acquisition of full data.

4.1 *Operation Time of Ring Scanning in the 3-D Track*

Here, the translation/revolution speed and moving time of the 3-D scanning mechanism are discussed to reach the working position in the radial, circular, and vertical directions, respectively.

4.1.1 *Radial movement*

The revolution speed (ω_r in deg/s) and moving time (t_r) of the rotating disk that transfers fiber channels to radial movement are expressed as

$$\omega_r = 6\Omega_{\mathrm{MA}} \times \varepsilon_r, \tag{4}$$

$$t_r = \alpha/\omega_r, \tag{5}$$

where Ω_{MA}, $\varepsilon_r = D_A/D_B$, and α are the revolution speed of motor A (in rpm), the speed ratio of belt pulley to rotating disk, and the driving angle (in deg), respectively; furthermore, the diameters (D_A and D_B) of the belt pulley and the rotating disk are 30 and 500 mm, respectively. In the design, provided that the speed of Ω_{MA} is set at 30 rpm, it drives the rotating disk at a speed of 10.8 deg/s owing to a speed ratio, ε_r, of 0.06. Therefore, it takes <2 s for the maximum α of 17 deg. In this scanning system, the maximum radial movement is 45 mm for all illumination or detection channels, and it can accommodate the tested breast ranging from 60 to 150 mm in diameter.

4.1.2 *Circular movement*

Similarly, the angular speed (ω_θ in deg/s) and its corresponding traveling time (t_θ) are expressed as

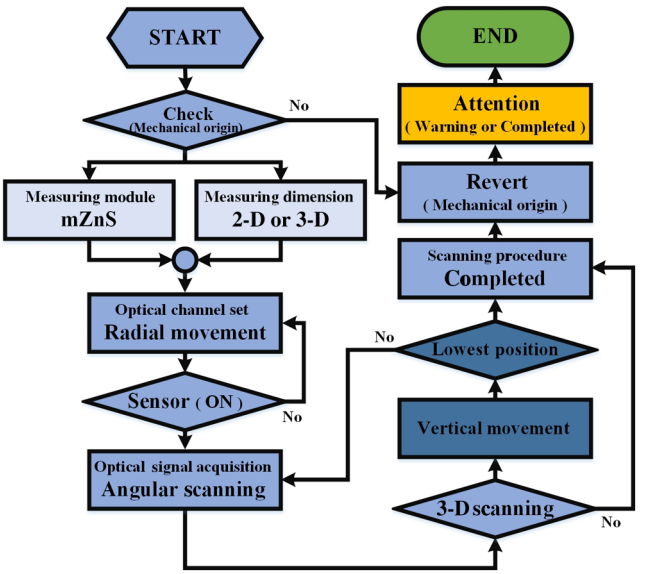

Fig. 11 Flow chart of mechanical and electro-optical control for the 3-D ring-scanning equipment.

$$\omega_\theta = 6\Omega_{\mathrm{MB}} \times \xi_r, \tag{6}$$

$$t_\theta = \theta/\omega_\theta, \tag{7}$$

where Ω_{MB}, ξ_r, and θ are the rotating speed of motor B (in rpm), the reduction ratio of a bevel gearbox, and the rotating angle (in deg), respectively. It takes 2 s for a rotating angle of 180 deg since the rotating speed is 90 deg/s provided that Ω_{MB} is 30 rpm with a reduction ratio of 1:2.

4.1.3 *Vertical movement*

The vertical speed (V_Z in mm/s) and time (t_Z) are expressed as

$$V_{\mathrm{Z}} = \frac{1}{60}\Omega_{\mathrm{MC}} \times l_Z, \tag{8}$$

$$t_{\mathrm{Z}} = L_Z/V_Z, \tag{9}$$

where Ω_{MC}, l_Z, and L_Z are the speed of motor C (in rpm), the lead of a ball screw (in mm/rev), and the stroke (in mm), respectively. For Ω_{MC} and l_Z of 30 rpm and 5 mm/rev, 0.4 s are required for each I mm in vertical movement.

According to the design, the total NIR data acquisition time of each slice (t_{slice}) will be <10 s provided that the output port of each detection channel is connected to a PMT, which is estimated from Eq. (10).

$$t_{\mathrm{slice}} = t_r + t_\theta + N_{\mathrm{scanning}} \times t_{\mathrm{sampling}}, \tag{10}$$

where the total time of the optical signal acquisition is $N_{\mathrm{scanning}} \times t_{\mathrm{sampling}}$; t_r is 1.57 s; t_θ and N_{scanning} for the 2Z3S configuration are 1.67 s and 5, respectively; and t_{sampling} is ~1 s when the scanning angle (θ) is equal to 150 deg. Thus, the total time of the entire procedure (t_{total}) for N scanned slices (N_{slice}) is estimated as in Eq. (11):

$$t_{\mathrm{total}} = N_{\mathrm{slice}} \times (t_{\mathrm{slice}} + t_Z). \tag{11}$$

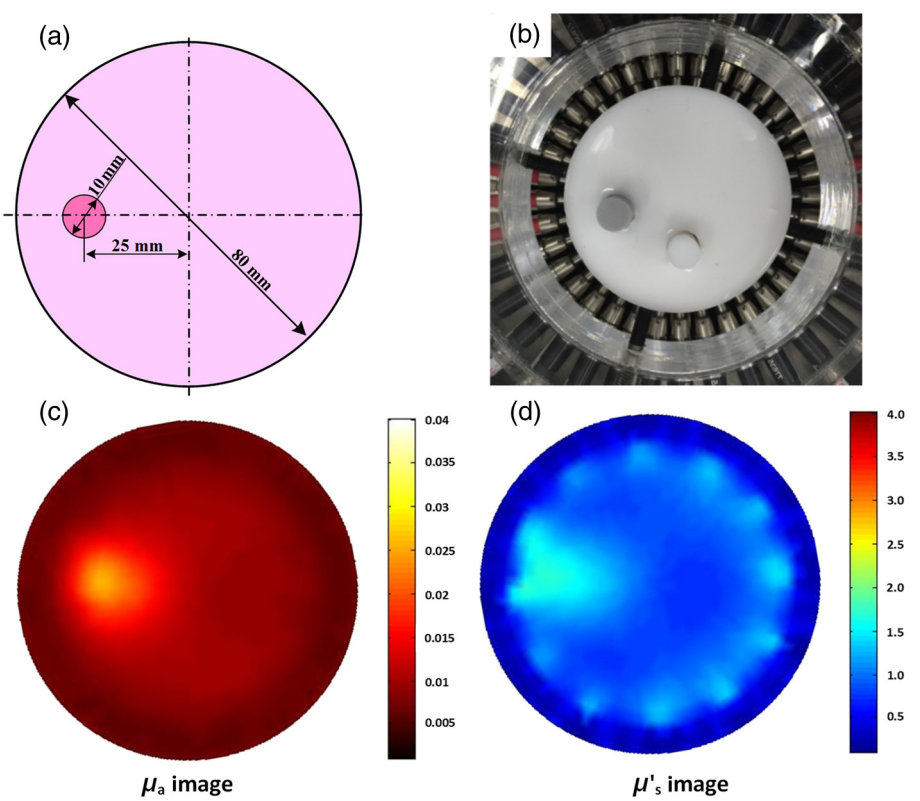

Fig. 12 Experimental trial validation: (a) schematic diagram of the tested phantom, (b) the tested phantom in our proposed scanning system, (c) the reconstructed μ_a image, and (d) the reconstructed μ_s' image.

4.2 *Flow Chart of System Control*

The design, machining, and operation of the proposed NIR DOI system have been described; moreover, the system control of mechanical motion and opto-electrical measurement plays a crucial role to steer the scanning system in a proper procedure. Figure 11 illustrates the procedure of mechanical motion and opto-electrical measurement that is coded through using LabVIEW™. As shown in Fig. 11, initial position of system is checked first, the measuring dimension within a specified measurement module is defined, and subsequently the scanning motion, optical illumination/detection, and data acquisition start. Following the radial motion of source/detection optical fiber channels reaching the breast/phantom as the limited sensors respond the detection, the NIR data are collected along with the angular motion of fiber channels at designated positions. Provided the scanning of 3-D mode was set, the vertical motion of optical channels carries on and optical data collection is completed for a full scanning cycle. At the end of measurement, the system returns to the reset/initial position to complete the procedure.

4.3 *Experimental Validation*

A phantom test was performed. We used amplitude-modulated (20 MHz) light as the illumination source from an 830 nm/10 mW NIR light generated from a laser diode since the difference between the absorptions of oxyhemoglobin/deoxyhemoglobin and lipid/water is significant at 830 nm, i.e., the former (0.1 to 1 mm^{-1}) is high and the latter (0.0001 to 0.001 mm^{-1}) is low. The phantom was made of silicone plus carbon and TiO_2 powders as absorption and scattering materials, respectively. A cylindrical phantom having an inner diameter of 80 mm was used as a background medium and a 10-mm-diameter tube containing different concentrations of carbon and TiO simulated an internal localized optical inclusion. The background medium had $\mu_a = 0.008\ mm^{-1}$ and $\mu_s' = 0.89\ mm^{-1}$, and a contrast level (2:1 for both μ_a and μ_s') between the inclusion and the background was used, where the inclusion was 25 mm off-centered and in the direction of 9 o'clock.

Figure 12 demonstrates the simultaneous reconstruction of both μ_a and μ_s' for an off-centered inclusion, where Figs. 12(a) and 12(b) show the schematic diagram and the tested phantom in the proposed scanning system, respectively, along with the reconstructed optical-property images in Figs. 12(c) and 12(d). As can be seen, the reconstructed images are quantitative with respect to the location and size of the object, although the artifact is obvious especially in the μ_s' image and the contrast was overestimated between the inclusion and the background.

5 Conclusion

With the aim of breast DOI, the study implemented a 3-D prostrate ring-scanning equipment with flexibly specified measuring modules; especially, its motion mechanism and driving details were addressed here. First, the image reconstruction for various synthesized scanning situations justified the proposed 3-D NIR ring-scanning equipment through (1) comparing with fixed-channel equipments and (2) sliced image reconstruction for the 3-D task. Unlike the fixed-channel configuration design, the proposed and implemented screening/diagnosing equipment has a flexibility for optical-channel expansion with a compromise among construction cost, operation time, and the spatial resolution of reconstructed μ_a and μ_s' images. As described, the radial motion of the designed system was driven by using a rotating disk platform associated with rotation-sliding-and-moving mechanism on which the mounted NIR sources and detectors are able to move simultaneously. Noncontact NIR data were acquired through three optical displacement sensors that are also employed to estimate image reconstruction profiles. This 3-D ring-scanning equipment remains being calibrated, and it is anticipated that anthropomorphic breast phantoms with physiological content[28] and clinical trials will be reported in the future.

Acknowledgments

This research was financially supported by the Ministry of Science and Technology in Taiwan through the grants 101-2221-E-008-093-MY3 and 101-2221-E-236-014.

References

1. D. B. Kopans, *Breast Imaging*, 2nd ed, Lippincott-Raven, Philadelphia (1998).
2. A. B. Hollingsworth et al., "Current comprehensive assessment and management of women at increased risk for breast cancer," *Am. J. Surg.* **187**(3), 349–362 (2004).
3. M. Herranz and A. Ruibal, "Optical imaging in breast cancer diagnosis: the next evolution," *J. Oncol.* **2012**, 863747 (2012).
4. J. P. Culvera et al., "Three-dimensional diffuse optical tomography in the parallel plane transmission geometry: evaluation of a hybrid frequency domain/continuous wave clinical system for breast imaging," *Med. Phys.* **30**(2), 235–247 (2003).
5. B. W. Pogue et al., "Instrumentation and design of a frequency domain diffuse optical tomography imager for breast cancer detection," *Opt. Express* **1**(13), 391–403 (1997).
6. R. Al abdi et al., "Optomechanical imaging system for breast cancer detection," *J. Opt. Soc. Am. A* **28**(12), 2473–2493 (2011).
7. S. M. W. Y. Van de Ven et al., "Optical imaging of the breast," *Cancer Imaging* **8**(1), 206–215 (2008).
8. S. B. Colak et al., "Tomographic image reconstruction from optical projections in light-diffusing media," *Appl. Opt.* **36**(1), 180–213 (1997).
9. S. B. Colak et al., "Clinical optical tomography and NIR spectroscopy for breast cancer detection," *IEEE J. Sel. Topics Quantum Electron.* **5**(4), 1143–1158 (1999).
10. F. E. W. Schmidt et al., "A 32-channel time-resolved instrument for medical optical tomography," *Rev. Sci. Instrum.* **71**(1), 256–265 (2000).
11. B. W. Pogue et al., "Quantitative hemoglobin tomography with diffuse near-infrared spectroscopy: pilot results in the breast," *Radiology* **218**(1), 261–266 (2001).
12. T. O. McBride et al., "Multispectral near-infrared tomography: a case study in compensating for water and lipid content in hemoglobin imaging of the breast," *J. Biomed. Opt.* **7**(1), 72–79 (2002).
13. S. Jiang et al., "Quantitative analysis of near-infrared tomography: sensitivity to the tissue-simulating precalibration phantom," *J. Biomed. Opt.* **8**(2), 308–315 (2003).
14. N. Iftimia et al., "A compact, parallel-detection diffuse optical mammography system," *Rev. Sci. Instrum.* **74**(5), 2836–2842 (2003).
15. T. D. Yates et al., "Time-resolved optical mammography using a liquid coupled interface," *J. Biomed. Opt.* **10**(5), 054011 (2005).
16. G. Gulsen et al., "Design and implementation of a multifrequency near-infrared diffuse optical tomography system," *J. Biomed. Opt.* **11**(1), 014020 (2006).
17. G. Gulsen et al., "Combined diffuse optical tomography (DOT) and MRI system for cancer imaging in small animals," *Technol. Cancer Res. Treat.* **5**(4), 351–363 (2006).
18. B. Alacam et al., "Pharmacokinetic-rate images of indocyanine green for breast tumors using near-infrared optical methods," *Phys. Med. Biol.* **53**(4), 837–859 (2008).
19. M. C. Pan et al., "Near infrared tomographic system based on high angular resolution mechanism—design, calibration, and performance," *Measurement* **42**(3), 377–389 (2009).
20. R. Padmaram, "The overall instrument design," Chapter 3 in *Design, Fabrication and Testing of a Versatile, and Low-Cost Diffuse Optical Tomographic Imaging System*, Master Thesis, pp. 30–65, Indian Institute of Science, Bangalore, India (2007).
21. X. Li et al., "Integrated diffuse optical tomography and photoacoustic tomography: phantom validations," *Biomed. Opt. Express* **2**(8), 2348–2353 (2011).

22. M. L. Flexman et al., "Digital optical tomography system for dynamic breast imaging," *J. Biomed. Opt.* **16**(7), 076014 (2011).
23. J. E. Gunther et al., "Using diffuse optical tomography to monitor tumor response to neoadjuvant chemotherapy in breast cancer patients," *Proc. SPIE* **8578**, 85780J (2013).
24. T. Yates et al., "Optical tomography of the breast using a multi-channel time-resolved imager," *Phys. Med. Biol.* **50**(11), 2503–2517 (2005).
25. J. M. Yu, M. C. Pan, and M. C. Pan, "Design for source-and-detector configuration of a ring-scanning-based near-infrared optical imaging system," *Opt. Eng.* **52**(1), 011002 (2014).
26. J. M. Yu et al., "Design of 3D ring-scanning mechanism for NIR diffuse optical imaging," presented at *Biomedical Optics, April 2014*, OSA, Miami, Florida (2014).
27. L. Y. Chen, M. C. Pan, and M. C. Pan, "Implementation of edge-preserving regularization for frequency-domain diffuse optical tomography," *Appl. Opt.* **51**(1), 43–54 (2012).
28. K. E. Michaelsen et al., "Anthropomorphic breast phantoms with physiological water, lipid, and hemoglobin content for near-infrared spectral tomography," *J. Biomed. Opt.* **19**(2), 026012 (2014).

Jhao-Ming Yu received his MS degree from the Institute of Mechanical and Electro-Mechanical Engineering, National Formosa University, Taiwan, in 2009. He is currently pursuing his PhD degree at the Department of Mechanical Engineering, National Central University, Taiwan. His research interests include various aspects of diffuse optical tomography, opto-mechatronics design, and illumination optical design.

Min-Cheng Pan received his BEng and MS degrees from National Chiao Tung University and National Taiwan University in 1988 and 1990, respectively, and his PhD degree in the Applied Optics Group of Department of Physics from the University of Reading, England, in 1999. He is currently a professor in the Department of Electronic Engineering, Tungnan University, Taiwan. His research interests include image restoration/super-resolution, image reconstruction, numerical method, electronic circuits and medical imaging systems, LED lighting design, and interdisciplinary research.

Ya-Fen Hsu received her MD degree from Taipei Medical University, Taiwan, in June 2002. She had her general surgery resident training and fellowship in Shin-Kong Memorial Hospital, Taipei, Taiwan, in 2003 and 2008. Now, she is serving as attending surgeon in Landseed Hospital, Taoyuan, Taiwan. Her research interests are breast cancer diagnosis and treatment. Previous research focused on cancer molecular biology.

Liang-Yu Chen received his PhD degree in mechanical engineering from the National Central University, Taiwan, in 2013. He is currently working in a postdoctoral position at the Graduate Institute of Biomedical Engineering, National Central University, Taiwan. His research interests include image reconstruction for diffuse optical imaging and numerical methods.

Min-Chun Pan received his PhD degree in mechanical engineering from KU Leuven in 1996. From 1996 to 1999, he was a senior researcher at Sanyang Industry Corporation and an adjunct associate professor in the Department of Forensic Science, Central Police University. Since 1999, he has been working with the Department of Mechanical Engineering, National Central University, as a full professor. His research interests are in the areas of DOT, medical devices design, and biomedical/mechanical signal processing.